INTERPLANETARY DOUBLE-SHOCK ENSEMBLES WITH ANOMALOUS ELECTRICAL CONDUCTIVITY

Murray Dryer

ABSTRACT

Similarity theory is applied to the case of constant velocity, piston-driven, shock waves. This family of solutions, incorporating the interplanetary magnetic field as developed by Lee and Chen for the case of infinite electric conductivity, represents one class of experimentally observed, flare-generated shock waves first described by *Hundhausen et al.* [1970]. This paper discusses the theoretical extension to flows with finite conductivity (presumably caused by unspecified modes of wave-particle interactions). Solutions, including reverse shocks, are found for a wide range of magnetic Reynolds numbers from one to infinity. Consideration of a zero and nonzero ambient flowing solar wind (together with removal of magnetic considerations) enables the recovery of the earlier similarity solutions of *Parker* [1963] and *Simon and Axford* [1966] as well as the numerical simulations of *Hundhausen and Gentry* [1969*a*]. For the magnetic case, it is shown that negligible joule heating occurs until the conductivity drops to more than 10 orders of magnitude below the solar wind's classical value of approximately $10^4\ (\Omega\text{–}m)^{-1}$. It is shown that even substantial joule heating has a negligible effect on the gross features of the double-shock ensemble. A limited comparison with observations suggests that flare energetics can be reasonably estimated once the shock velocity, ambient solar wind velocity and density, and ambient azimuthal Alfvén Mach number are known.

INTRODUCTION

Early speculations and theoretical studies of interplanetary shock waves [*Parker*, 1963] were quickly confirmed by spacecraft observations (for several excellent reviews, see *Hundhausen*, 1970*a*, *b*). It is now well known that Alfvén waves as well as discontinuities on large (> 0.01 AU) and small (< 0.01 AU) scale lengths, respectively, exist in the solar wind [*Burlaga*, 1968, 1971; *Belcher et al.*, 1969]. This paper is concerned with a theoretical study of shock waves and contact surfaces. Such ensembles were suggested [*Carmichael*, 1962; *Sonett and Colburn*, 1965] to be responsible for sudden commencements, positive and negative magnetic impulses, and substorms. On the basis of simultaneous solar wind and ground observations, *Hirshberg et al.* [1970*a*, *b*] suggest, that contact surfaces following a number of shock waves may be associated with substorms and may be identified by an enriched α-particle abundance presumably traceable back to the flare plasma itself. Since Sonett and Colburn's suggestion that these two discontinuities should be followed by a rearward-facing (or reverse) shock wave, a number of theoretical and experimental studies have examined this ensemble.

Sturrock and Spreiter [1965] considered the forward-reverse shock ensemble from a steady-state point of view without consideration of the magnetic field. By considering Hugoniot conditions, they arrived at a class of allowable configurations for what might be called the "shock-tube" analogy in one-dimensional, ordinary gas-dynamics. This study was extended by *Schubert and Cummings* [1967, 1969] who included a transverse

The author is at the Space Environment Laboratory, National Oceanic and Atmospheric Administration, Environmental Research Laboratories, Boulder, Colorado.

magnetic field in an infinitely conducting plasma. In comparing their analysis with a potential experimental (Mariner 2) candidate for an ensemble [*Neugebauer and Snyder,* 1967], they showed that the peak in the proton density did lead the peak in the magnetic field strength as predicted by their shock jump calculations. Because of the time-invariant aspect, however, their study precluded any temporal variation. This suggested identification must therefore be considered inconclusive.

Time dependence was explicitly considered for the forward shock by *Parker* [1963], who employed similarity theory without consideration of the magnetic field or the kinetic energy of the undisturbed, ambient solar wind. A prominent feature of this spherically symmetric solution was the infinite value of density at the position of the contact discontinuity, or "piston." *Korobeinikov and Nikolayev* [1970] have referred to a similar solution. *Simon and Axford* [1966] extended this similarity solution to include the flow that extends from the "piston" back to the reverse shock. The transverse magnetic field was explicitly considered for an infinitely conducting fluid by *Lee and Chen* [1968] and extended by *Dryer* [1970] and *Eviatar and Dryer* [1970] to the case of a fluid with finite conductivity. Significantly, these latter solutions also considered the *explicit* presence of the undisturbed solar wind through which the forward shock moves with arbitrary speed as described by *Lee* [1965]. *Lee et al.* [1970] then proceeded to extend the infinitely conducting solution to the flow between the "piston" and the reverse shock. This paper reexamines the study performed earlier [*Dryer,* 1970] and extends the entire ensemble (comprising the reverse shock, contact discontinuity, and forward shock) so that it includes the more physically realistic presence of finite conductivity.

Related studies including consideration of the ambient solar wind but without the magnetic field were made by *Hundhausen and Gentry* [1969*a, b*]. Their numerical simulation studies considered the superposition of arbitrary disturbances (initiated at 0.10 AU) on a typical steady solar wind model. They concluded that a flare that continues to exert a constant momentum, hence a linear (with time) increase of energy, on the "piston" for longer than ~5 hr would produce the double-shock ensemble, which would persist to earth's orbit. Conversely, they showed that rarefaction waves emanating from the flare extend to the propagating reverse shock and thereby weaken and eventually cause it to disappear when the flare ceases its activity prior to 5 hr. Thus, they further suggested that the ensemble would rarely be observed at 1 AU.

Experimental observations of the double shock are inconclusive. *Hundhausen et al.* [1970], for example, report observations of a number of piston-driven shocks but make no identification of possible associated reverse shocks. One might conclude that the latter were dissipated prior to their arrival at 1 AU. It is known, however, that reverse shocks must exist. *Burlaga* [1970] reports the first unambiguous indentification of a reverse shock on 18 September 1967 by using simultaneously measured plasma and field data from Explorer 34 instruments. Identification of a piston, or *contact discontinuity,* and forward shock as part of a possible ensemble, however, was not attempted. *Hundhausen* [1970*b*] has suggested that *Lazarus et al.* [1970] may have observed an ensemble on 11 August 1967; he also reports the possible identification of a reverse shock, using Vela 4B plasma data only, on 5 July 1967. It is of great interest to note that the first interplanetary shock ever observed [by Mariner 2; *Sonett et al.,* 1964] on 7 October 1962, as mentioned above, *may* have been part of ensemble as suggested by *Schubert and Cummings* [1967, 1969]. Also, the suggestion by *Hirshberg et al.* [1970*a, b*] that the contact discontinuity might be identified by the anomalous He^{++}/H^{+} abundance may prove useful.

It is clear, then, that further study, both theoretical and experimental, is required to provide unambiguous evidence, including simultaneous magnetic field measurements, of this class of flare-generated shock waves.

Additional, but still limited, evidence of piston-driven shocks has been given by the VLF electric field observations of Pioneers 8 and 9 [*Scarf et al.,* 1970; *Scarf and Siscoe,* 1971; and *Siscoe et al.,* 1971]. These authors have suggested that significant wave-particle interactions occur for a substantial time scale (hr) following the passage of interplanetary shock waves. *Dryer* [1970] has shown, as a result, that associated anomalous electrical conductivity could be incorporated into the theory. The presence of nonclassical resistivity has already been discussed from several points of view [*Sagdeev,* 1967; *Speiser,* 1970], which include stochastic "collisions" of electrons with fluctuating electric fields and even "non-noise" effects due to electron inertial effects.

Here we first demonstrate the character of the piston-driven shock for a wide range of magnetic Reynolds numbers (that is, anomalous electrical conductivity) as a basis for estimating how low σ should be before significant departure from the infinitely conducting solution takes place. A second purpose is to examine a typical double-shock ensemble from the theoretical point of view for both $\sigma = \infty$ and $\sigma \neq \infty$.

ANALYSIS

The nomenclature used for the piston-shock problem is identical to that used in the basic problem considered by Parker (fig. 1). It should be noted that the deformed magnetic field illustrated for the spherical model in figure 1 indicates the presence of a *contact* discontinuity

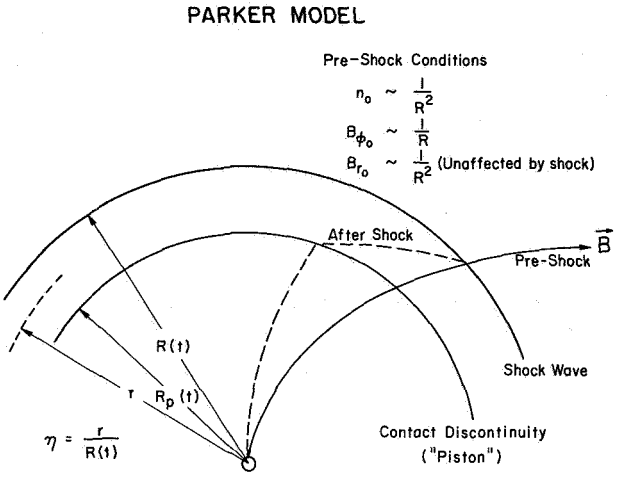

Figure 1. *Sketch and nomenclature of the shock wave-piston combination as proposed originally by Parker [1963]. The special case of a constant velocity combination gives rise to a reverse shock (not shown here) which follows the piston.*

(as distinguished from the tangential and rotational types) at the piston; that is, there is a component of **B** normal to the piston. More realistic nonspherical configurations, however, may require a *tangential* discontinuity over most of its surface [*Hundhausen,* 1971]. The reverse shock, which causes another kink in the field, is not shown.

The time-dependent partial differential equations, including the Lorentz force, joule heating, and magnetic diffusion, are given in figure 2. Except for the use of Ampere's law on the right side of the energy equation, these equations are identical to those used in the earlier study [*Dryer,* 1970], which considered the electric field in an explicit way. Figure 3 shows the equations [*Lee and Chen,* 1968] that are used to transform the equations into ordinary differential equations. The boundary conditions at the shock and piston are also shown. The crossed-out terms in the jump conditions are permitted under the assumption that the inverse of the transverse ambient Alfvén Mach number (squared) is

$$\frac{\partial \rho}{\partial t} + \frac{\partial(\rho u)}{\partial r} + \frac{2\rho u}{r} = 0$$

$$\frac{\partial u}{\partial t} + u\frac{\partial u}{\partial r} + \frac{1}{\rho}\frac{\partial p}{\partial r} = -\frac{1}{\rho\mu} B_\phi\left(\frac{\partial B_\phi}{\partial r} + \frac{B_\phi}{r}\right) \quad \text{(MKSQ UNITS)}$$

$$C_v\left(\frac{\partial}{\partial t} + u\frac{\partial}{\partial r}\right)\ln p\rho^{-\gamma} = \frac{1}{\rho T}\frac{J^2}{\sigma} = \begin{cases} \frac{\sigma}{\rho T}\left(\bar{E} + \bar{V}\times\bar{B}\right)^2 \\ \frac{1}{\rho T \sigma \mu^2}\left(\nabla\times\bar{B}\right)^2 \end{cases}$$

$$\frac{\partial B_\phi}{\partial t} + \frac{1}{r}\frac{\partial}{\partial r}(ruB_\phi) = \frac{1}{\mu\sigma}\left(\frac{\partial^2 B_\phi}{\partial r^2} + \frac{2}{r}\frac{\partial B_\phi}{\partial r}\right)$$

Where: $\bar{V} = (u, o, o)$

$\bar{B} = (B_r, o, B_\phi)$

$\bar{E} = (o, E_\theta, o)$

Figure 2. *Basic time-dependent equations of mass, momentum, energy conservation and induction for a finitely conducting plasma which is permeated by a magnetic field. Gravitational attraction to the sun is negligible and therefore neglected. Thermal conduction and viscosity are not considered.*

TRANSFORM P.D.E. TO O.D.E. BY USING THE FOLLOWING SIMILARITY TRANSFORMATIONS (LEE & CHEN):

$\rho = \rho_0\,\psi(\eta)$

$u = (V-u_0)\,\phi(\eta)$

$p = \gamma^{-1}\rho_0 (V-u_0)^2 f(\eta)$

$B_\phi = B_{\phi_0}\, b(\eta)$

$\eta = \frac{r}{R(t)}$

Where: $V = \frac{dR}{dt}$ = Shock Velocity

u_0 = Undisturbed Solar Wind Velocity

BOUNDARY CONDITIONS:

At Shock:

$$[\rho u] = 0$$

$$\left[\rho u^2 + p + \frac{B_\phi^2}{2\mu}\right] = 0$$

$$\left[\rho u v_\phi - \frac{B_r B_\phi}{\mu}\right] = 0$$

$$\left[\frac{\gamma}{\gamma-1}\frac{p}{\rho} + \frac{1}{2}(u^2 + v_\phi^2) + \frac{B_\phi^2}{\mu\rho} - \frac{B_r B_\phi}{\mu\rho} v_\phi\right] = 0$$

$$[B_r] = 0$$

$$[uB_\phi - v_\phi B_r] = 0$$

At Piston:

$$u_p = \frac{dR_p}{dt} = \frac{d[\eta_p R(t)]}{dt} = \eta_p V$$

$$\phi_p = \left(\frac{V}{V-u_0}\right)\eta_p = k\,\eta_p$$

Figure 3. *Similarity transformation equations and boundary conditions for a double-shock ensemble which propagates into an ambient plasma which moves radially with a velocity u_0. The crossed-out terms in the shock jump equation may be omitted if $M_{A_\phi}^{-2} < 1.0$.*

small compared to one. It is also important to note that the parameter $k = V/(V-u_0)$ allows consideration of any shock velocity V superimposed on a solar wind of velocity u_0. The value $k = 1$ reproduces the similarity solutions (neglecting the Lorentz force, joule heating,

and induction equation) found by *Parker* [1963] and *Simon and Axford* [1966]. The reverse shock problem is solved by noting that V_R (the reverse shock velocity) is less than the new value of the solar wind velocity u_0 through which it is moving, and thus $k < 1$; whereas the forward shock (*velocity* = V_F) problem is solved for $\eta \leq 1$ the reverse shock problem is solved for $n \geq 1$ as noted by *Lee* [1965]. The latter solution is then "folded over" to match the discontinuity where the pressures and velocities must be matched in this "two-point" boundary-value problem.

The ordinary differential equations are given in figure 4 which also gives the definitions of the transverse Alfvén Mach number and magnetic Reynolds number.

$$(k\eta-\phi)\frac{\psi'}{\psi}-\phi'+\frac{2(k\eta-\phi)}{\eta} \overset{\text{O. D. E.}}{=} 0 \qquad ,(\ )'=\frac{d(\ )}{d\eta}$$

$$(k\eta-\phi)\psi\phi'-\frac{1}{\gamma}f'-M_{A_\phi}^{-2}b\left(b'+\frac{b}{\eta}\right)=0$$

$$(k\eta-\phi)\left[\frac{f'}{f}-\frac{\gamma\psi'}{\psi}\right]-2k(\gamma-1) = \begin{cases} -\gamma\left[(\gamma-1)\left(1-\frac{E_\theta}{uB_\phi}\right)^2\right]R_M M_{A_\phi}^{-2}\frac{(\phi b)^2}{f} \\ -\gamma(\gamma-1)R_M^{-1}\,M_{A_\phi}^{-2}\frac{1}{f\eta^2}\left[(\eta b)'\right]^2 \end{cases}$$

$$(k\eta-\phi)\frac{b'}{b}-\phi'+\frac{k\eta-\phi}{\eta} = -R_M^{-1}\left[\frac{b''}{b}+\frac{2b'}{\eta b}\right]$$

Where: $k=\frac{V}{V-u_0}$ = Constant

$M_{A_\phi}=\frac{V-u_0}{B_{\phi_0}/(\mu\rho_0)^{1/2}}$ = Constant

$R_M = R(V-u_0)\mu\sigma$ = Constant or $R_M(\eta)$

Figure 4. *Ordinary differential equations which result when the transformation shown in figure 3 is applied to the partial differential equations in figure 2. Note that M_{A_ϕ} must be constant as required by the radial dependence of B_{ϕ_0} and ρ_0, hence the constancy of V-u_0. The lower (equivalent) joule heating term is used in this paper. A perfect gas with polytropic exponent γ is assumed.*

The upper term on the right side of the energy equation (containing the electric field explicitly) was considered in the earlier work [*Dryer*, 1970]. It was found, however, that numerical instabilities were introduced when the product $(\gamma-1)\ (1-E_\theta/uB_\phi)^2 R_M$ exceeded 100. The results discussed in this paper are found with the use of the *lower* expression on the right side of the energy equation. Further details are given in the appendix.

The earlier solutions examined the introduction of anomalous conductivity near the piston [*Dryer*, 1970], as well as near the forward shock [*Eviatar and Dryer*, 1970]. The present results (noting the persistent, disturbed conditions behind shocks as observed by the VLF electric field measurements) assume the conductivity to be less than classical *everywhere* between the piston and the two shocks (thus, R_M is taken as constant within this region). Similarity is therefore maintained from a mathematical sense; from a physical view, the fact that $R \sim$ time requires that $\sigma \sim (\text{time})^{-1}$. It is not known if the latter requirement (namely, that the conductivity at a given η decreases with time) is justified on physical grounds. The following results, however, are found assuming that the restrictions (spherical symmetry, applicability to the vicinity of the solar equatorial plane, $\sigma \sim t^{-1}$) are not important in the determination of basis features of the double-shock problem.

RESULTS

Nondimensional Parameters between the Piston and Forward Shock

The effect of k is shown in figure 5 for a typical case

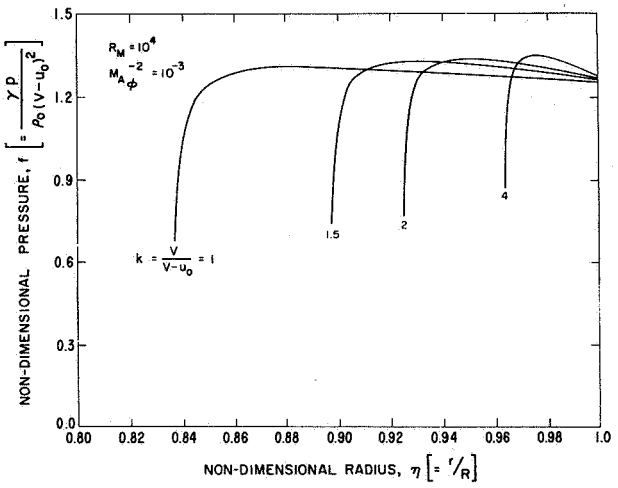

Figure 5. *The effect of the relative velocity between the forward shock and solar wind velocities on the nondimensional pressure distribution, f, for anomalous electrical conductivity ($R_m = 10^4$, $M_{A_\phi}^{-2} = 10^{-3}$).*

where $M_{A_\phi}^{-2} = 10^{-3}$ and $R_M = 10^4$. The nondimensional pressure f is shown to achieve a physically meaningful value for $k = 1.0$, 1.5, 2.0, and 4.0. It is recalled that the pressure goes to zero at the piston (the minimum value of η for each case) when the fluid is infinitely conducting [*Lee and Chen*, 1968]. The polytropic

exponent $\gamma = 5/3$ is used for all of the calculations in this paper.

The effect of finite conductivity (again for the pressure) is shown in figure 6 for the special case $k = 2$.

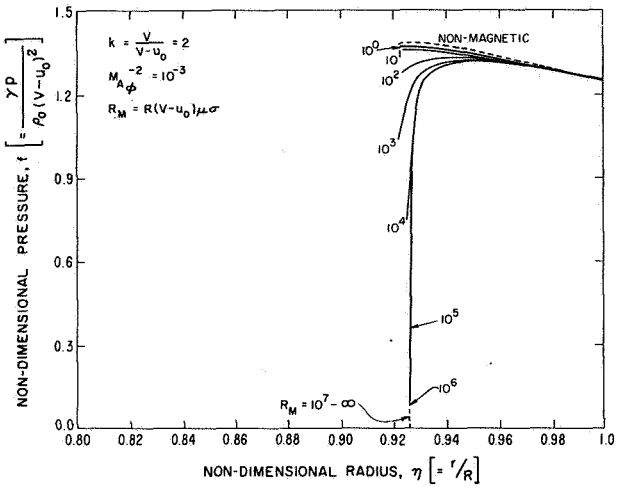

Figure 6. *The effect of anomalous conductivity on the nondimensional pressure distribution f for k = 2. Note that the nonphysical result for infinite electrical conductivity is gradually eliminated as the conductivity is first assumed to be classical (at 1 AU and a typical relative velocity of 100 km sec^{-1}, $R_m = 10^{14}$) and then increasingly "anomalously" low. The nonmagnetic case is shown as the limiting pressure distribution for k = 2, $M_{A_\phi}^{-2} = 0$, and $\gamma = 5/3$.*

The result noted above for infinite conductivity is shown. A similar result, hardly discernible from the case where $\sigma = \infty$, is found when a classical value ($\sigma = 10^4$ mhos m^{-1}) is taken for typical solar wind conditions wherein $R_M = 10^{14}$ at 1 AU. A decrease of eight orders of magnitude produces a small, but finite, pressure at the piston. However, more realistic piston pressures are found with additional decreases of the conductivity. The result for the limiting nonmagnetic case was found by considering the equations of motion without the magnetic terms or induction equation; the *Parker* [1963] and *Simon and Axford* [1966] solutions are recovered when $k = 1$.

The nondimensional density results for ψ are shown in figure 7, again for $k = 2$. The infinite density at the piston for the nonmagnetic case is clearly shown. Significant decreases are shown at the piston for the cases of infinite and anomalous conductivities. Note that finite, but still large, density increases (a factor of 20 over the ambient value) at the piston are found by the nonmagnetic numerical solutions [cf. *Hundhausen and Gentry*, 1969*b*]. The important role of the magnetic field is suggested by the results for moderately low values of σ in figure 7.

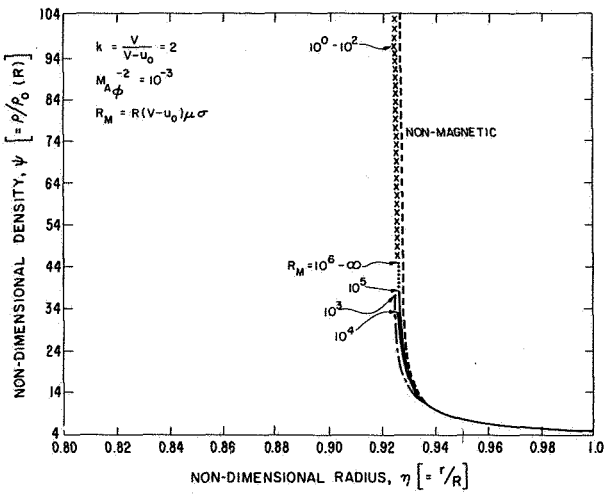

Figure 7. *The effect of anomalous conductivity on the nondimensional density distribution f for k = 2. The density is infinite at the piston for the nonmagnetic case, reminiscent of the same result for k = 1 found by Parker [1963] and Simon and Axford [1966]. Conversely, the density is finite at the piston for the case of infinite conductivity [Lee and Chen, 1968]. The nonmagnetic case is recovered as the conductivity approaches zero.*

The nondimensional magnetic field is shown in figure 8 where we note that maximum joule heating will be

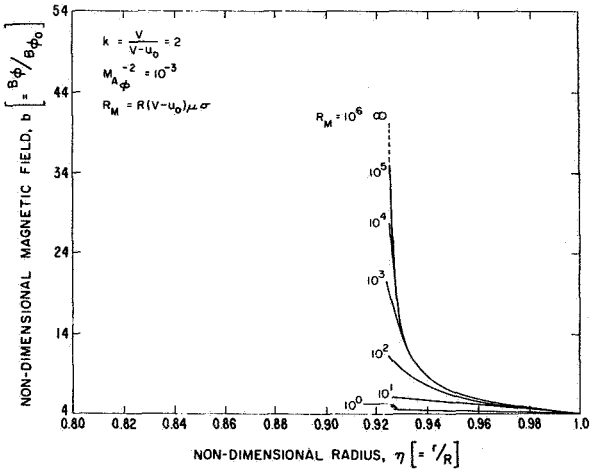

Figure 8. *The effect of anomalous conductivity on the nondimensional azimuthal magnetic field distribution b for k = 2.*

expected near the piston. The expected rise in temperature is clearly demonstrated in figure 9. The non-

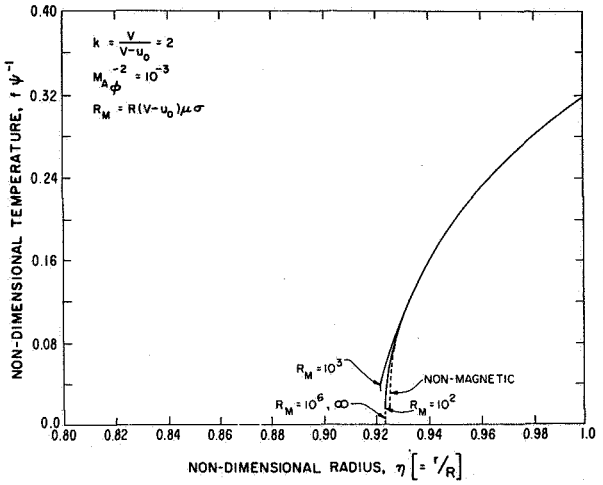

Figure 9. *The effect of anomalous conductivity on the nondimensional temperature distribution $f\psi^{-1}$ for $k = 2$.*

dimensional velocity is shown in figure 10 where no change is seen in the magnitude of the convective velocity when the conductivity is decreased by many orders of magnitude. This velocity insensitivity is anticipated since the joule heating is expected to affect the relative magnitudes of the magnetic and thermal energy densities with a minor effect on the kinetic energy density.

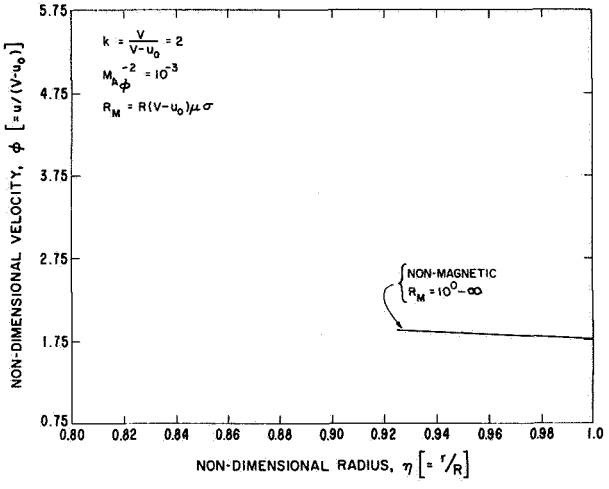

Figure 10. *The effect of anomalous conductivity on the nondimensional velocity distribution ϕ for $k = 2$.*

Energy Budget

The relative energies in the disturbed plasma are now examined explicitly for the flow between the forward shock and the piston. Figure 11 shows the integral for the three energies—kinetic, thermal, and magnetic—contained between these two boundaries and formed within a unit solid angle of 1 steradian. The second and

$$E(t) = \int_{r_p}^{R(t)} \left[\frac{1}{2}\rho u^2 + \frac{p}{\gamma-1} + \frac{B_\phi^2}{2\mu} \right] r^2\, dr \;/\text{STERADIAN}$$

$$= \rho_0\, R^3\, (V-u_0)^2\, L$$

$$\text{Where } L = \int_{\eta_p}^{1} \left[\frac{\psi\phi^2}{2} + \frac{f}{\gamma(\gamma-1)} + \frac{b^2}{2M_{A\phi}^2} \right] \eta^2\, d\eta$$

$$= \text{FUNCTION OF } (k, M_{A\phi}, R_M)$$

Figure 11. *Energy integral for the sum of kinetic, thermal, and magnetic energies contained between the piston and the forward shock. A similar integral, not given here, may be written for the disturbed plasma between the reverse shock and the piston.*

third lines in the figure are found by applying the similarity transformations given in figure 3. The parameter L is seen to be a function of k, M_{A_ϕ}, and R_M. For a given shock observation, the energy is found directly once the following parameters are measured: the ambient transverse field $B_\phi{}^0$, the shock velocity V, ambient solar wind velocity u_0, ambient density ρ_0, and, of course, the forward shock position R. A similar calculation is made for the flow between the piston and the reverse shock to complete the total energy contained within the disturbed plasma and thus equal to the mechanical energy released during the flare process.

The energy budgets for several values of $M_{A_\phi}^{-2}$ (10^{-2}, 10^{-3}) are given for $1 \leq R_M \leq \infty$ and $k = 1.0$, 1.5, 2.0, and 4.0 in figures 12, 13, 14, and 15, respectively. The nonmagnetic result is shown on the left side of each figure for comparison. Of greatest interest is the observation that the electrical conductivity must be reduced (say, at 1 AU, from the 10^4 mhos m^{-1} figure mentioned previously) by more than 6 orders of magnitude before the joule heating can effectively raise the thermal energy density at the expense of the magnetic. In fact, further reduction of this anomalous conductivity causes even the kinetic energy density to decrease by several percent.

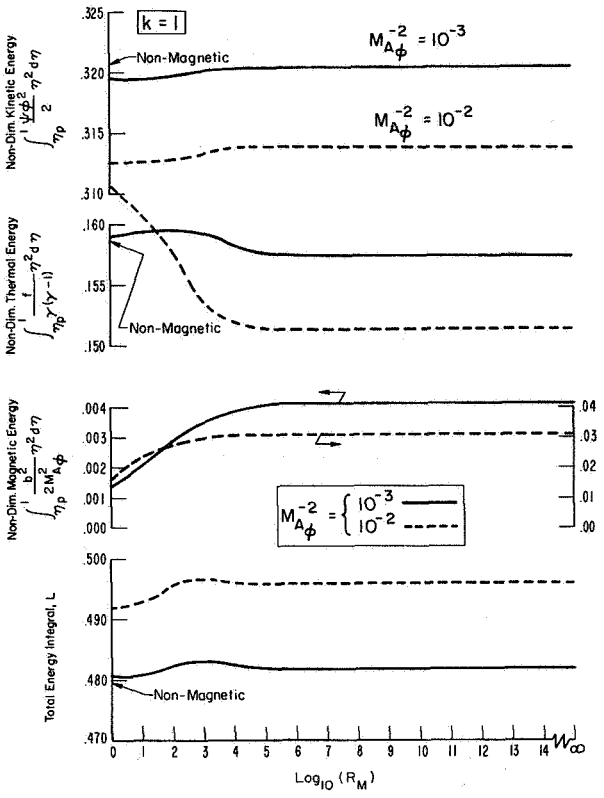

Figure 12. *The effect of magnetic Reynolds number on the energy budget within the piston–forward-shock combination for several values of* $M_{A\phi}^{-2}$ *when there is no solar wind (k = 1).*

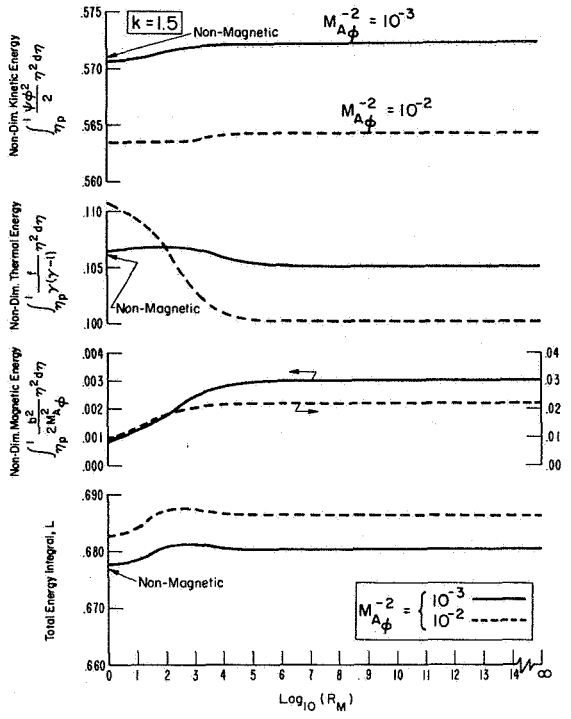

Figure 13. *The effect of magnetic Reynolds number on the energy budget within the piston–forward-shock combination for several values of* $M_{A\phi}^{-2}$ *when k = 1.5.*

A second observation is also of interest: for the hypothetical case of $u_0 = 0$—that is, $k = 1$—the nonmagnetic budget shows that the ratio of kinetic energy density to thermal energy density is 2:1. This ratio shifts predominately in favor of the kinetic energy when $k > 1$; that is, when the solar wind is turned on so that the ambient flux is "shocked" and incorporated into the budget of the disturbed flow. A third observation is concerned with the range of this computation's validity: as $M_{A\phi}^{-2}$ approaches 1, the need to consider the transverse equation of momentum arises as discussed by *Lee and Chen* [1968]. As a result, the present solution is expected to be valid to values of $M_{A\phi}^{-2}$ as high as 10^{-1} after which L diverges rapidly.[1]

[1] *In this connection, figure 6 and table II of Dryer [1970] are in error for values of* $M_{A\phi}^{-2}$ other than 10^{-3}. *As shown here (figs. 12-15), the value of L increases slowly at first as* $M_{A\phi}^{-2}$ *is increased.*

The kinetic energy flux in the disturbed plasma has been experimentally measured between the forward shock and the piston (and, possibly, behind it in some cases where the data are inconclusive) by *Hundhausen et al.* [1970] for a number of shocks (approximately six events). Their results for two of these cases are shown on the right side of figure 16. Also shown, for comparison, are the theoretical results (which include the thermal and magnetic energies) found by neglecting the possible presence of the disturbed flow between the piston and the reverse shock. Note that agreement is good for the 15 February 1967 shock but not for the 18 December 1965 shock. It is possible that the discrepancy is due to the decreased validity of the theory because $M_{A\phi}^{-2}$ is close to 1; an additional contributing factor may be the lack of detailed data during the early years of plasma measurements.

Double-shock Structure

"Snapshots" of the nonmagnetic double-shock structure have been presented by *Hundhausen and Gentry*

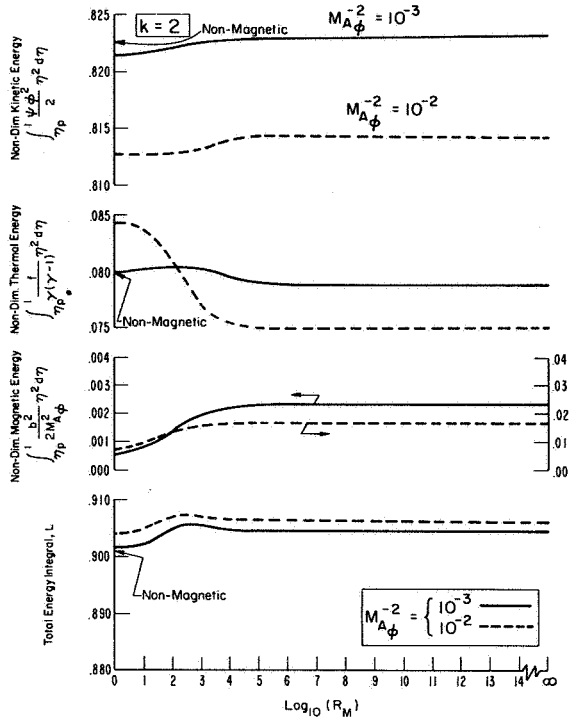

Figure 14. *The effect of magnetic Reynolds number on the energy budget within the piston–forward-shock combination for several values of* $M_{A\phi}^{-2}$ *when* $k = 2$.

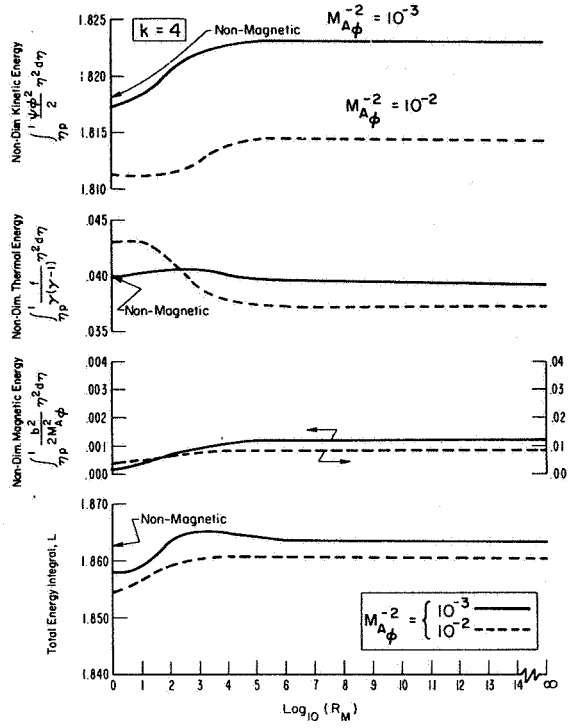

Figure 15. *The effect of magnetic Reynolds number on the energy budget within the piston–forward-shock combination for several values of* $M_{A\phi}^{-2}$ *when* $k = 4$.

[1969*a*] and compared with the similarity results of *Simon and Axford* [1966] in a more detailed study [*Hundhausen and Gentry,* 1969*b*]. The analysis discussed above is now extended to relax the earlier similarity assumptions of (1) zero solar wind velocity and (2) nonmagnetic considerations. The assumption of negligible thermal energy density in the ambient solar wind (both in front of the forward shock and in the "new" solar wind which follows the reverse shock) is retained in view of the dominant presence of the kinetic energy flux.

For the purpose of presenting additional "snapshots" (in the present case, spatial distributions of all parameters as a function of the nondimensional radius $\eta = r/R$), a specific candidate for a double-shock structure is chosen. The case in point is concerned with the 29 August 1966 shock reported by *Chao* [1970] and others. This case is chosen only in order to provide typical values of ambient number density and velocity n_0 and u_0, forward shock velocity V, and azimuthal magnetic field component B_{ϕ_0}, which are required by the theory. A detailed comparison of the experimental (plasma and field) data with the theory is presently nearing completion [*Dryer et al.,* 1971]. The present discussion is limited to the theoretical results for the spatial distribution of all parameters as a function of nondimensional radius η.

Shock	Reference	k	$M_{A\phi}$	R_M	L	E ERGS	$(E)_{EXP.}$ ERGS
18 Dec'65	Hundhausen, Bame, & Montgomery (1970), JGR Taylor, (1969) Solar Phys.	3.4	1.2	10^{14}	1.5	5×10^{31}	1.4×10^{31}
15 Feb '67	Hirshberg et al. (1970) JGR Hundhausen (1970) Ann. Geophys.	2.2	6.6	10^{14}	.95	11×10^{31}	9×10^{31}

Figure 16. *Comparison of theoretical and experimental estimates for the energy in the disturbed plasma caused by two flares. E is found from the equation in figure 11 and the experimentally determined parameters listed above, assuming classical conductivity.* $(E)_{Exp}$ *includes only the kinetic energy flux [Hundhausen et al., 1970]. (Assumed: Solid angle =* π *ster)*

The following values were found from data provided by *N. F. Ness* and *J. H. Wolfe* [private communications] and *Chao* [1970]: $n_0 = 4.0$ cm^{-3}, $u_0 = 345$ km sec^{-1}, $V = 467$ km sec^{-1}, and $B_{\phi_0} = 0.74\gamma$. The shock velocity is almost identical with that found by *Hundhausen* [1970*a*, p. 470]. Thus, $k = 3.83$ and $M_{A_\phi}^{-2} = 4.41\times10^{-3}$; and the polytropic exponent γ, is assumed to be 5/3 for this example. Infinite electrical conductivity and a low value of anomalous conductivity are examined.

The flow between the piston and forward shock is directly found by the method and parameters noted above. The second part of the flow in our "two-point" boundary value problem is determined uniquely once the "new" solar wind values of density and ambient magnetic field are specified behind the reverse shock. The "new" solar wind is assumed to obey the "old" requirements: $n_0 \sim r^{-2}$ and $B_{\phi_0} \sim r^{-1}$. Thus, we are free to specify new constants of proportionality under the restriction that: (1) the density in the new coronal expansion will be greater than its original value had the disturbance not come by [cf. *Hundhausen and Gentry*, 1969*b*]; and (2) the hotter coronal base condition will require a higher plasma velocity, which in turn will cause the magnetic topology to become more nearly radial. Hence B_{ϕ_0} will be less than its original value at the same (as yet undetermined) position. The new constants of proportionality, then, are arbitrarily chosen to be twice and 2/3 the original values for the density and azimuthal magnetic field components, respectively, for this example. An iterative computation is then performed until the essential boundary conditions at the common piston are satisfied: equality of total pressures and velocity on contiguous sides of the piston. The final results of this iteration produce a new solar wind velocity, $u_0 = 519$ km sec^{-1}, within which the reverse shock velocity propagates outward at a velocity of 437 km sec^{-1}. (The familiar analogy is that of the child who tries to walk unsuccessfully *down* an "up" escalator and arrives at the top at a later time than his brother who decides to walk *up* the moving stairs.) The resulting values of k and $M_{A_\phi}^{-2}$ are -5.34 and 2.18×10^{-3}, respectively, for the reverse shock-piston part of the flow.

The spatial distributions of velocity, density, thermal pressure, temperature, and azimuthal magnetic field are given as a function of the nondimensional radius η in figures 17, 18, 19, 20, and 21, respectively. Note that the disturbed plasma occupies a region of space $0.935 \leq \eta \leq 1.00$, which represents nearly 20 percent of the volume encompassed by the forward shock at any time for the combination of the three parameters: k, $M_{A_\phi}^{-2}$ and γ given above. When finite conductivity is

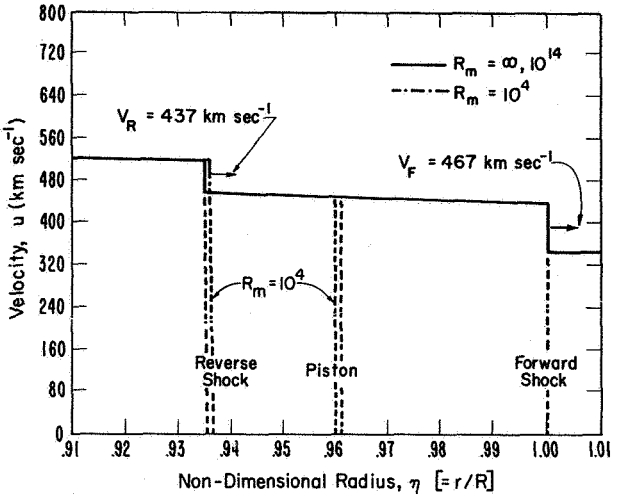

Figure 17. *Velocity distribution within the double-shock ensemble described in the text. V_F and V_R refer to the forward and reverse shock velocities, respectively. The values shown here refer to the time when the forward shock was first detected by Pioneer 7 on 29 August 1966 at R = 1.01 AU. Note the imperceptible change (shown in exaggerated form) in piston and reverse shock positions when R_m is reduced. The reverse shock velocity, found as part of the iterative procedure, is insensitive to the degree of anomalous conductivity chosen for the piston-reverse shock computation.*

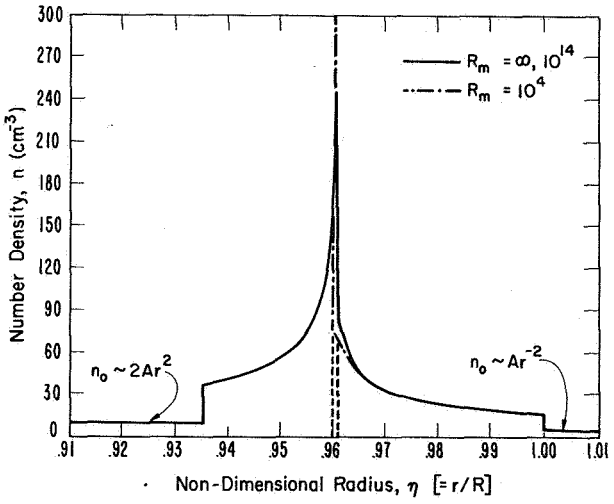

Figure 18. *Number density distribution within the double-shock ensemble described in the text. A is a constant of proportionality for the undisturbed solar wind.*

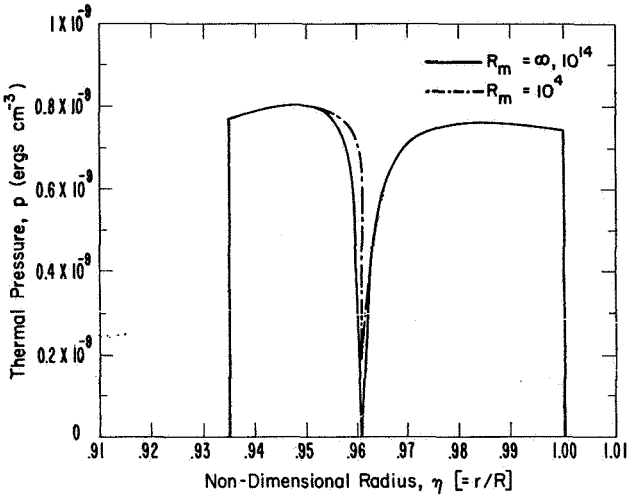

Figure 19. *Thermal pressure distribution within the double-shock ensemble described in the text. Note that anomalous electrical conductivity removes the nonphysical pressure at the piston.*

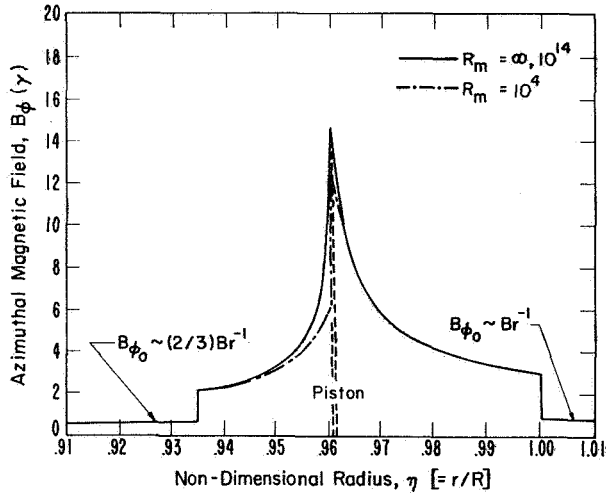

Figure 20. *Temperature distribution within the double-shock structure described in the text. Note that anomalous electrical conductivity removes the nonphysical temperature at the piston.*

"turned on," the piston moves slightly rearward and the reverse shock moves imperceptibly forward as shown in slightly exaggerated form in figure 17.

Several general comments are made with respect to each plasma parameter. In figure 17 it is seen that the velocity jump (~100 km sec^{-1}) at the forward shock is followed by a very gradual increase until the reverse shock is encountered. A smaller velocity change is seen at the latter position. Figure 18 shows, for infinite con-

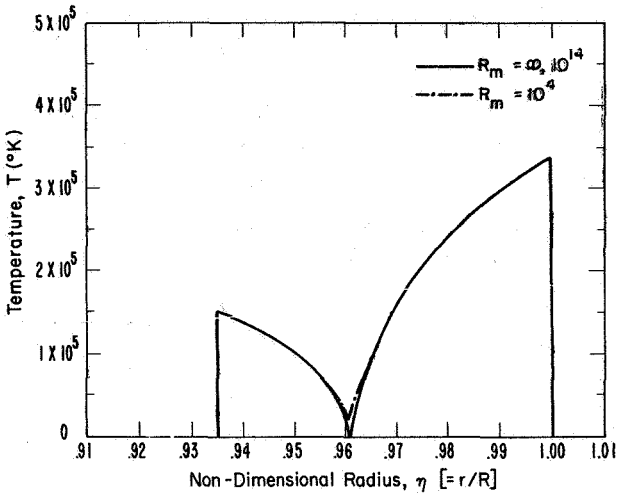

Figure 21. *Azimuthal magnetic field magnitude within the double-shock ensemble described in the text. Note that β (=p/(B²/2μ)) contiguous to the piston on the reverse shock's "side" is greater by nearly an order of magnitude then its value on the forward shock's "side." The sums of the two pressures, however, are identical at the piston itself, as required. "B" is a constant of proportionality for the undisturbed solar wind ahead of the forward shock wave.*

ductivity, a precipitous density increase on the reverse shock's "side" of the piston. Figures 19 and 20 (for the infinite-conductivity case) show the nonphysical zero pressure and temperature, respectively, at the piston. The assumption of anomalous conductivity, however, removes this physically unrealistic condition. Figure 21 shows a maximum compression of the azimuthal magnetic field on both sides of the piston where the topology of the field approaches that for a contact discontinuity, as suggested in figure 1. When the electrical conductivity, is decreased by 10 orders of magnitude, however, the peaks of *all* precipitous changes of thermodynamic and magnetic properties at the piston are still present. One expects that thermal conduction and viscous dissipation would change this picture. The piston "boundary layer" would be expected to be "smeared" with the introduction of these additional transport properties, as in the case of earth's magnetopause. As noted earlier, work presently in progress [*Dryer et al.*, 1971] compares these results with experimental data (for a double-shock candidate) observed by an essentially inertial observer (Pioneer 7). A statistically valid test of the theory, however, will require a much larger experimental sample than those discussed herein as well as in the existing literature on piston-driven shocks.

CONCLUDING REMARKS

It has been shown that similarity theory can be applied to constant velocity, double-shock wave ensembles with explicit consideration of the interplanetary magnetic field and ambient solar wind kinetic energy flux. It has also been shown that nonphysical results for thermal pressure and temperature at the piston for the case of infinite electrical conductivity were removed in a gradual way by permitting the introduction of an increasingly larger degree of anomalous electrical conductivity within the shocked plasma. The consequent joule heating produces significant conversion from magnetic to thermal energy when the conductivity decreases by more than 10 orders of magnitude below the classical value. Other anomalous transport properties, such as thermal conductivity and [collisionless] coupling of various species, may also be present; but no consideration of these possibilities has been taken into account. Furthermore, there is no requirement (in this magnetogasdynamic analysis to specify the nature of the mechanism(s) required for the anomalous conductive property. It is theoretically possible to determine, indirectly, the order of magnitude of the anomalous conductivity by making detailed measurements of all plasma parameters. These measurements would be made either at an inertially stationary observation point (as a function of time) or at a number of radially spaced points (preferably located within a unit solid angle of π steradians centered at the sun and including the responsible flare).

In this connection, the conductivity level might be inferred from the level of the density and magnetic field magnitudes in the vicinity of the piston, which in turn may include a rich supply of alpha particles as a last vestige of the flare itself [*Hirshberg et al.*, 1970*a*, *b*]. The problem of unambiguous identification of reverse shocks has been pointed out by *Burlaga* [1970] since they are expected to be weaker than forward shocks and diffusive in their gross structure [*Hundhausen et al.*, 1970]; as a result, their identification requires detailed information (high resolution) on both plasma and field.

It is noted by *Hirshberg et al.* [1970*b*] that most of the piston-driven shocks in their study (identified by high alpha/proton abundances) exhibited shock velocities at 1 AU that were about 0.8 the average speed required by tentative flare-shock time delays. The implication is that these shocks moved outward from the sun at nearly constant velocity; hence the present assumption of constant velocity is justified. A more serious limitation of the theory is the spherically symmetric assumption. Criticism of this assumption would indeed be justified if measurements of a particular ensemble were made near the boundaries of a highly collimated ejection. Measurements near the central radius of the flare, however, would be expected to be amenable to comparison with theory inasmuch as the effect would be equivalent to a spherical ejection as noted by *DeYoung and Hundhausen* [1971], who performed numerical studies of nonspherical, nonmagnetic blast waves. Also, at least one remarkable west-limb event observed by the Culgoora 80-MHz radioheliograph on 30 March 1969 [*Smerd*, 1970] gave rise to an unambiguous shock-associated type II burst that clearly exhibited a greater-than-180° extent projected on a plane perpendicular to the line of sight. It is not known, of course, if this was a unique event or whether similar events are common.

Finally, comparison of magnetic field and density distributions for the complete ensemble (figs. 18 and 21) shows that an inertial observer would first see a peak in the former followed by a peak in the latter parameter. This result differs from the time-independent analysis of *Schubert and Cummings* [1969].

ACKNOWLEDGMENTS

It is a pleasure to thank N. F. Ness and J. H. Wolfe for the use of their unpublished data, and G. H. Endrud for programming the equations on the computer. Discussions with T. S. Lee and T. Chen were very beneficial and are gratefully acknowledged.

APPENDIX: Computational Details

Here we briefly summarize essential details involved in the solution of the transformed equations of motion and the induction equation. The basic equations, with the usual symbols for the dependent variables, are shown in figure 2. The transformation equations are given in figure 3. The boundary conditions at the shock, neglecting the ambient internal energy, are:

$$f(\eta_s) = \frac{2\gamma}{\gamma + 1} \tag{A1}$$

$$\psi(\eta_s) = \frac{\gamma + 1}{\gamma - 1} \tag{A2}$$

$$\phi(\eta_s) = k - \frac{\gamma - 1}{\gamma + 1} \tag{A3}$$

$$b(\eta_s) = \frac{\gamma + 1}{\gamma - 1} \tag{A4}$$

The equations are integrated from the shock η_s to the piston position η_p. The latter is found when $\eta_p = \phi/k$ (fig. 3).

The transformed equations are shown in figure 4 where the single and double primes indicate ordinary first and second derivatives, respectively, with respect to

η. Some comments are now made for the two cases of infinite and finite electrical conductivity:

Solution for the Infinite-Conductivity Case

The infinite conductivity case is formed from the basic equations when $R_m = \infty$. The equations then take the following form:

$$\phi' = \frac{2f}{\eta\gamma} \frac{\gamma\alpha - \eta k(\gamma-1)}{M_{A_\phi}^{-2} b^2 + f - \alpha^2 \psi} \tag{A5}$$

$$b' = \frac{b}{\alpha} [\phi' - \frac{\alpha}{\eta}] \tag{A6}$$

$$\psi' = \frac{\psi}{\alpha} [\phi' - \frac{2\alpha}{\eta}] \tag{A7}$$

$$f' = \frac{f}{\alpha} [2k(\gamma-1) + \gamma(\phi' - \frac{2\alpha}{\eta})] \tag{A8}$$

where $\alpha = k\eta - \phi$, and $\eta_s = 1$ at the shock wave.

A Runge-Kutta fourth-order technique was used to integrate this set of equations. The same basic procedure was used for both the forward and the reverse shock calculations with one exception: $k < 1$ for the reverse shock, so that problem was solved for $\eta \geq 1$. For the reverse shock case, values for the shock velocity and the solar wind velocity behind the shock were iterated until the bulk velocity and the total pressure matched the same parameters for the forward shock case at the piston. The reverse shock solution was then translated to match the forward shock at the piston.

Solutions for the Finite-Conductivity Case

The equations are second order and nonlinear in b in the finite conductivity case; thus, a boundary condition for b' is required, No independent relationship for b' is known, so an approximation was made by solving for b' in terms of b'':

$$b' = \frac{b\phi' - \frac{\alpha b}{\eta} - \frac{b''}{R_M}}{\alpha + (2/R_M\eta)} \tag{A9}$$

This equation is the same as (A6) in the infinite conductivity case when $R_M \to \infty$.

Reasonable values of b'', as suggested by results from the infinite conductivity case, were substituted into (A9) to provide the required boundary condition. For lower values of R_M, values of b'' were selected to provide a smooth change in all variables between the limiting cases of infinite conductivity an nonmagnetic flow.

The Runge-Kutta fourth-order solution of the second-order set of equations proved to be unstable for high values of R_M. An approximate solution was obtained by a first-order solution for b with $b' = b'(b'')$ [eq. (A9), using the value of b'' from the previous step in the calculations]. This approximate solution corresponded very closely with the infinite conductivity case at $R_M = 10^{14}$.

No such approximation was made for solutions with low values of R_M. To reduce the truncation error, however, a Ricatti transformation [$b' = \epsilon b$] was applied. For the reverse shock case, the two solutions matched at $R_M = 10^6$.

The same basic procedure used in the infinite conductivity case was applied to calculate the reverse shock and to match total pressures and bulk velocities at the piston. Total CDC 3800 computer time is less than 4 min for the complete double-shock ensemble.

REFERENCES

Belcher, J. W.; Davis, L. Jr.; and Smith, E. J.: Large Amplitude Alfvén Waves in the Solar Wind. *J. Geophys. Res.*, Vol. 74, 1969, p. 2302.

Burlaga, L. F.: Micro-scale Structures in the Interplanetary Medium. *Solar Phys.*, Vol. 4, 1968, p. 67.

Burlaga, L. F.: A Reverse Hydromagnetic Shock in the Solar Wind. *Cosmic Electrody.*, Vol. 1, 1970, p. 233.

Burlaga, L. F.: Discontinuities and Shock Waves in the Interplanetary Medium and Their Interaction with the Magnetosphere. *Proc. Leningrad Symp. Solar-Terrest. Phys.*, May 11-20, 1970, D. Reidel Publishing Company, Dordrecht-Holland, 1971 (in press).

Carmichael, H.: Discussion following paper by A. J. Dessler, Hydromagnetic Picture of Earth Storms. *J. Phys. Soc. Japan*, Vol. 17 (Supp. A-II), 13, 1962. (Proc. Int. Conf. Cosmic Rays and the Earth Storm, Kyoto, 4–15 Sept. 1961).

Chao, J. K.: Interplanetary Collisionless Shock Waves. *Massachusetts Institute of Technology Report CSR TR-70-3*, February 1970.

DeYoung, D. S.; and Hundhausen, A. J. : Non-spherical Propagation of a Flare-Associated Interplanetary Blast Wave. *J. Geophys. Res.*, Vol. 76, 1971, p. 2245.

Dryer, M.; Smith, Z. A.; Endrud, G. H.; and Wolfe, J. H.: Some Observations of the August 29, 1966, Interplanetary Shock Wave by Pioneer 7, (abstract). *E⊕S Trans., Amer. Geophys. Union*, Vol. 52, 1971, p. 336.

Dryer, M.: Some Effects of Finite Electrical Conductivity on Solar Flare-Induced Interplanetary Shock Waves. *Cosmic Electrodyn.*, Vol. 1, 1970, p. 348.

Eviatar, A.; and Dryer, M.: Finite Conductivity and Interplanetary Piston-Driven Shock Waves. *Cosmic Electrodyn.*, Vol. 1, 1970, p. 371.

Hirshberg, J.; Alksne, A.; Colburn, D. S.; Bame, S. J.; and Hundhausen, A. J.: Observation of a Solar Flare Induced Interplanetary Shock and Helium-Enriched Driver Gas.. *J. Geophys. Res.*, Vol. 75, 1970*a*, p. 1.

Hirshberg, J.; Asbridge, J. R.; and Robbins, D. E.: The Helium-Enriched Interplanetary Plasma from the Proton Flares of August/September, 1966 (abstract). *E⊕S Trans. Amer. Geophys. Union*, Vol. 51, 1970*b*, p. 818.

Hundhausen, A. J.: Composition and Dynamics of the Solar Wind Plasma. *Rev. Geophys. Space Phys.*, Vol. 8, 1970*a*, p. 729.

Hundhausen, A. J.: Solar Wind Disturbances Associated with Solar Activity. *Intercorrelated Satellite Observations Related to Solar Events* (Proc. Third ESLAB/ESRIN Symp. Noordwijk, The Netherlands, Sept. 16-19, 1969), edited by V. Manno and D. E. Page, D. Reidel Publishing Company, Dordrecht-Holland, 1970*b*.

Hundhausen, A. J.; and Gentry, R. A.: Numerical Simulation of Flare-Generated Disturbances in the Solar Wind. *J. Geophys. Res.*, Vol. 74, 1969*a*, p. 2908.

Hundhausen, A. J.; and Gentry, R. A.: Effects of Solar Flare Duration on a Double Shock Pair at 1 AU. *J. Geophys. Res.*, Vol. 74, 1969*b*, p. 6229.

Hundhausen, A. J.: Interplanetary Shock Waves and the Structure of Solar Wind Disturbances. Presented at the Solar Wind Conference, Asilomar, California, 21-26 March 1971. (this volume).

Hundhausen, A. J.; Bame, S. J.; and Montgomery, M. D.: Large-Scale Characteristics of Flare-Associated Solar Wind Disturbances. *J. Geophys. Res.*, Vol. 75, 1970, p. 4631.

Korobeinikov, V. P.; and Nikolayev, Yu. M.: Shock Waves and Magnetic Field Configurations in Interplanetary Space. Symp. Solar-Terrestrial Physics, Leningrad, USSR, May 11-20, 1970 (abstract I 4-7).

Lazarus, A. J.; Ogilvie, K. W.; and Burlaga, L. F: Interplanetary Shock Observations by Mariner 5 and Explorer 34. *Solar Phys.*, Vol. 13, 1970, p. 232.

Lee, T. S.: Unsteady Flows in an Unsteady Environment. *Phys. Fluids*, Vol. 8, 1965, p. 1266.

Lee, T. S.; and Chen, T.: Hydromagnetic Interplanetary Shock Waves. *Planet. Space Sci.*, Vol. 16, 1968, p. 1483.

Lee, T. S.; Chen, T.; and Balwanz, W. W.: Hydromagnetic Theory for Disturbances Following an Ideal "Solar Thermal Explosion" (abstract). *E⊕S Trans. Amer. Geophys. Union*, Vol. 51, 1970, p. 414.

Neugebauer, M.; and Snyder, C. W.: Mariner 2 Observations of the Solar Wind; 2: Relation of Plasma Properties to the Magnetic Field. *J. Geophys. Res.*, Vol. 72, 1967, p. 1823.

Parker, E. N.: *Interplanetary Dynamical Processes.* Chap. 8, 1963, Interscience Publishers, New York.

Sagdeev, R. Z.: On Ohm's Law Resulting from Instability. *Magneto-Fluid and Plasma Dynamics, Proc. Symp. in Applied Mathematics*, Vol. 18, 1967, p. 281.

Scarf, F. L.; Green, I. M.; Siscoe, G. L.; Intriligator, D. S.; McKibbin, D. D.; and Wolfe, J. H.: Pioneer 8 Electric Field Measurements in the Distant Geomagnetic Tail. *J. Geophys. Res.*, Vol. 75, 1970, p. 3167.

Scarf, F. L.; and Siscoe, G. L.: The Pioneer 9 Electric Field Experiment: Part 2, Observations between 0.75 and 1.0 AU. *Cosmic Electrodyn.*, Vol. 2, 1971,.

Schubert, G., and Cummings, W. D.: The Double Shock Wave Structure in the Solar Wind. *J. Geophys. Res.*, Vol. 72, 1967, p. 5275.

Schubert, G.; and Cummings, W. D.: Effect of High Electron-Proton Temperature Ratios on the Double Shock Wave Structure in the Solar Wind. *J. Geophys. Res.*, Vol. 74, 1969, p. 897.

Simon, M.; and Axford, W. I.: Shock Waves in the Interplanetary Medium. *Planet. Space Sci,.* Vol. 14, 1966, p. 901.

Siscoe, G. L.; Scarf, F. L.; Green, I. M.; Binsack, J. H.; and Bridge, H. S.: Very-Low-Frequency Electric Fields in the Interplanetary Medium: Pioneer 8. *J. Geophys. Res.*, Vol. 76, 1971, p. 828.

Smerd, S. F.: Radio Evidence for the Propagation of Magnetohydrodynamic Waves Along Curved Paths in the Solar Corona. *Proc. ASA*, Vol. 1, 1970, p. 305.

Sonett, C. P.; and Colburn, D. S.: The SI^+ -SI^- Pair and Interplanetary Forward-Reverse Shock Ensemble. *Planet. Space Sci.*, Vol. 13, 1965, p. 675.

Sonett, C. P.; Colburn, D. S.; Davis, L., Jr.; Smith, E. J.; and Coleman, P. J., Jr.: Evidence for a Collision-Free Magnetohydrodynamic Shock in Interplanetary Space. *Phys. Rev. Lett.*, Vol. 13, 1964, p. 153.

Speiser, T. W.: Conductivity Without Collisions or Noise. *Planet. Space Sci.*, Vol. 18, 1970, p. 613.

Sturrock, P. A.; and Spreiter, J. R.: Shock Waves in the Solar Wind and Geomagnetic Storms. *J. Geophys. Res.*, Vol. 70, 1965, p. 5345.

DISCUSSION *A. Hundhausen* There's one problem, in the choice of the data chosen. One expects a reverse shock because there is a flow from behind which is catching up with something already out in front of it. It seems you picked data where, in general, the velocity is decreasing with time. That would seem to me a rather highly unlikely candidate for a reverse shock.

M. Dryer That was quite right. We picked this as something to get our feet wet. I have data (not shown) which indicates the kinetic energy flux calculated the way you have suggested in the paper with Bame and Montgomery and indeed the kinetic energy flux does decrease with time. So this may have been—probably was—a blast wave.

D. S. DeYoung Did you include gravitational effects in your, symmetry solution?

M. Dryer No.

D. S. DeYoung So your temperature in the ambient medium before the shock arrives has to be zero; is that right?

M. Dryer That's right, and after the reverse shock has gone.

COMMENTS

D. S. DeYoung I have a brief report on some calculations similar to those introduced this afternoon by Art Hundhausen. He described nonspherically symmetric numerical simulations of flare associated disturbances propagating into the interplanetary medium. All the calculations he discussed were done in a blast wave limit, which in this context means that the duration of the disturbance was much less than the propagation time to 1 AU and that the energy in the disturbance remained constant after initialization. I would like to discuss briefly some additional results obtained from essentially the same numerical method but which explore initial conditions other than this blast wave limit. The geometry is the same as previously discussed with spherical symmetry in the ambient solar wind and an axisymmetric flare associated disturbance. The most obvious case opposite to a blast wave is, of course, a driven disturbance. Such a case was simulated in an ambient solar wind identical to the one used for the blast calculations, a wind with a radial velocity at 1 AU of 400 km/sec, a number density of 12 and a temperature of about 3.5×10^4 °K, again at 1 AU. The same half-angle of 15° was subtended by the initial cone of disturbance material so that comparison could be made with the blast wave case. The driven disturbance (driven here really should be in quotation marks) is initialized as follows: The shock velocity was set at 1000 km/sec at 0.1 AU just as in the blast wave case, but as the disturbance then propagated outward in a radial direction, a flux of material was maintained flowing outward across the innermost radial boundary, again at 1000 km/sec. This outflow kept on until the shock front associated with the disturbance reached 1 AU; it is in this sense that I meant "driving" to be in quotation marks—that is, we have no piston, we are really just leaving the disturbance turned on, and it is thus not "driven" in the classical sense.

It should be remembered that leaving the disturbance turned on for such a long time represents an extreme case, and one would not expect to find such an event actually occurring on the sun. The transit time to 1 AU for this disturbance is about 40 hours, which gives a total mass for this event of 10^{17} grams and a total kinetic energy of about 10^{32} ergs. This is the mass and energy contained in the disturbance when its associated shock front reaches 1 AU.

The driven case arrives at 1 AU in about two-thirds the time required for the comparable blast wave. The radial velocity along the disturbance symmetry axis decreases most rapidly at small heliocentric distances for both the blast and the driven case, but the amount of deceleration is quite different. By the time the shock wave reaches 1 AU for the blast wave case the shock velocity is half its initial value, whereas the driven shock suffers only a 25 percent loss. The deceleration of both disturbances is strongest at small heliocentric distances because of the strong radial dependence of the ambient solar wind

density, which produces the greatest momentum transfer from the front to the ambient medium in regions close to the sun.

The decrease in transit time for the driven case can be understood in terms of the increased mass and energy present in the disturbance. These two parameters also affect the shape of the shock front at 1 AU in that they determine whether the dynamics of the disturbance at 1 AU is dominated by momentum or by pressure. It is useful to calculate the so-called equal mass radius, which is the distance from the sun at which the mass of the ambient solar wind contained in the disturbance cone is equal to the total amount of mass we have injected into the disturbance by the time the front passes 1 AU. If this radius is much less than 1 AU we expect the disturbance to have transferred most of its momentum to the ambient solar wind, to have been slowed considerably, and to have the shock front propagating more or less uniformly in all directions due to a high, uniform pressure behind the front. This is just what is seen in the blast wave case, with its slow-moving, broad shock front at 1 AU. If the equal mass radius is of the order of 1 AU, then the front is expected to be more rapidly moving, to be propagating primarily due to the directed momentum of the ejected flare associated material, and for the front to be more narrow and streamlined. This is what is seen in our driven case here. Although there is always some uncertainty in the angle subtended by the cone of disturbance material, for the driven case the cone angle is between 30° and 45°, giving and equal mass radius of about 0.8 AU. Another factor which contributes to a narrower shock front at 1 AU is the decrease in transit time of the driven disturbance, which allows less time for the hot, high pressure material directly behind the strong shock front to undergo expansion transverse to the original motion of the ejected material.

Another possible initial condition for a flare-associated disturbance is that in which the flare produces simply a hot region of gas at base of the corona. This material would not have an extraordinarily large radial velocity; in fact, it would share the same radial velocity and possibly the same density as the ambient solar wind, but it would simply be hotter. This condition can be simulated with the present method, and was done so with the same ambient solar wind and with the same half-angle for the cone subtended by the disturbance. In this case we inserted at 0.1 AU a disturbance of the same density and radial velocity as in the steady state solar wind but increased the temperature by a factor of 10, giving a temperature in the disturbed region of 10^7 deg. Having so initialized the situation, the disturbance was allowed to freely propagate upwards as this warm level rose in the solar wind. The results are shown in figure 1.

The total energy in this disturbance is 10^{30} ergs, though it's mostly in the form of heat. This energy is not totally out of reason when compared to energies derived by other means. Note that the front takes a long time to reach 1 AU, and that when it does so, it is again roughly spherically shaped, but the center of the sphere tends to lie much more closely to the solar point rather than at some point further out along the symmetry axis. This may or may not imply poor agreement with observations, because there are certain irregularities in the shape, but certainly this is a broader front than one gets with either the driven or the blast wave case.

The heated bubble is an extremely low velocity disturbance, which is essentially convected out with the ambient solar wind. The transit time of this disturbance to 1 AU is generally in excess of what is usually thought. I recall a transit time of around 55 hr as being much more typical. Here the transit time is more like 73 hr.

Figure 2 shows a blast wave case with a disturbance containing 25 percent helium. The same initial energy was used, so that the initial shock velocity is a little less. What happens here is exactly what one would expect. There is early deceleration, perhaps not quite as strong due to the greater momentum per unit mass of the disturbance, but there are no real surprises here. What one would want to investigate next, I think, is a driven case with helium in the driving gas, to see what differences would result.

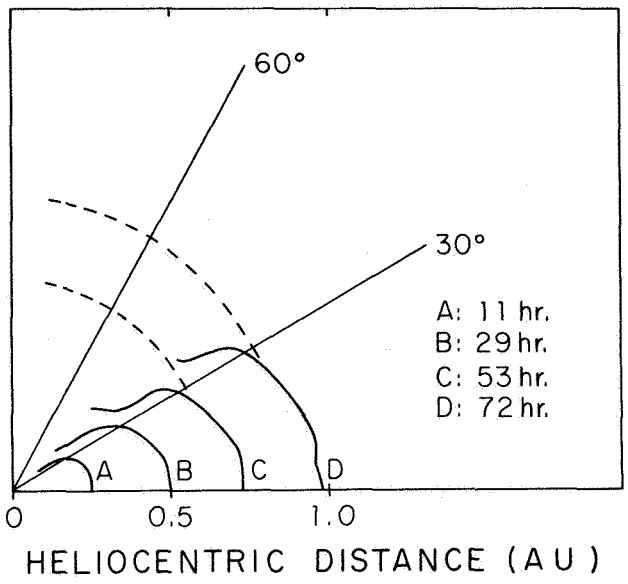

Figure 1. *Shock front shape as a function of heliocentric distance for the thermally initiated disturbance. The times shown are hours elapsed since release of the disturbance at 0.1 AU. The dashed lines are reference circles centered on the sun, and the symmetry axis is along the bottom of the figure.*

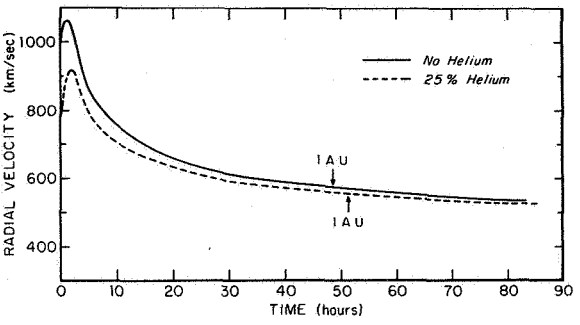

Figure 2. *Radial velocity of the shock front along the symmetry axis as a function of elapsed time for disturbances with and without* He. *The arrows indicate the time at which the disturbance passes 1 AU. The ambient solar wind speed at 1 AU is 400 km/sec*$^{-1}$.

DISCUSSION *J. Hirshberg* In comparing these calculations with observations you assume that the solar wind is spherically symmetric, while in the real case we have fast streams in the sectors, so we don't really expect to see these shapes very easily in any particular case.

D. S. DeYoung Yes. That's particularly true for disturbances that are of low initial energy and tend to be convected out with the ambient solar wind, where they can be highly distorted by any inhomogeneities that exist there.

G. Newkirk How formidable a job would it be to include the magnetic field in a couple of very simple configurations?

D. S. DeYoung I don't know what your scale of formidability is. It would not be too easy.

G. Newkirk Would it exceed your patience?

D. S. DeYoung Probably not.

G. Newkirk The configurations one would want would be where the event is collimated by the field or by the magnetic bubble.

D. S. DeYoung It would require major revisions in the code, but I don't think it's beyond the pale of one's imagination to do so in time.

G. Newkirk One of the things we know about flares is that they are associated very closely with the magnetic field.

M. Dryer I think it might be possible to take a magnetic field, just the line with the local velocity vector. It's completely artificial because the magnetic field in theory doesn't affect the flow. It would be the same kind of calculation John Spreiter and I have done for the interaction of the solar wind with the magnetosphere.

Would you agree to that, John?

J. Spreiter Not wholly. It is true that if the flow is steady, and the field is alined with the flow in, say, the oncoming stream, it will remain alined everywhere else, but the flow quantities are affected by the magnetic field. In particular, in some ranges of Mach

number and Alfvén Mach number, the hydromagnetic flow may be very different from the related gasdynamic flow. In fact, you can even have instances in which the MHD flow looks like gasdynamic flow going the other way; in other words, Mach waves extend upstream instead of downstream. For high Alfvén Mach number, however, the MHD and gasdynamic flows may not look terribly different.

A. J. Hundhausen One thing I advise in judging formidability is that the calculations we have done here are entirely in the range where the kinetic energy in the flow dominates. The real interest in magnetic channeling is done very low down in the corona where the ambient flow is subsonic and it may be quite a different problem.

D. S. DeYoung It is possible that you could match up these two regimes. You could do a low beta calculation close down where the field is high, then match it to this type later on.

W. I. Axford In this bubble business you have to really let the bubble go right from the bottom, I'm afraid, because you're depending very much on the potential energy of the bubble. If you let it already go from 20 $R_\odot$, which is where you started, there is essentially no potential energy left. What you've got to play with is the gravitational energy or the escape energy of all the gas that the bubble takes up. At the bottom of the corona where the velocity is 600 km/sec, if you're sharing that among fewer particles you've got a very large amount of energy to play with. But if you start higher the escape velocity decreases to ~100 km/sec, so there is really no source of energy available to give the buoyancy.

D. S. DeYoung Yes, but there is so little to run into that I think the density gradient in the ambient solar wind will result in a lot of transverse expansion anyway; it may present a much more nearly spherical front centered on the sun.

W. I. Axford That's true. It's a very complicated problem. That's why I hope you're doing it again. But the problem is rather like having a balloon and if you want to get it to pop out of the atmosphere you grease it very well and then start it at the bottom, not halfway up, or perhaps like a cork in a barrel; if you really want the cork to pop out of the water you pull it way down and then you let it go; you don't start it near the surface.

COMMENTS

E. J. Smith The other day I presented some results from a study of sector boundaries that we are carrying out using Mariner 5 magnetometer data. Another aspect of the study deals with the physical characteristics of the sector boundary, specifically the changes in the plasma and magnetic field observable at high time resolution. There have been discussions of vector boundaries over the past few days on several occasions and I thought some of you might like to see what they look like close up.

This aspect of the analysis is much less well developed than the results I presented the other day, so I want to add a word of caution. First of all, I'm just going to show how the magnetic fields change across the sector boundary. Furthermore, I have selected for presentation a certain subset of sector boundaries which have some particularly interesting structure; I don't want to leave the impression that these are necessarily the only type of sector boundaries to be found. On the other hand, the boundaries to be shown are frequently occurring. I would estimate that we see them in over half the cases studied. As will be seen, we have studied enough examples to be able to prepare some histograms.

Figure 1 deals with the magnitude of field changes. In carrying out this analysis we have been particularly interested in determining the extent to which the properties of the sector boundaries are like the neutral sheet in the earth's magnetotail with which everyone nowadays is familiar. I have chosen three examples of the magnetic field magnitude and a histogram is shown below. As you will notice, these are for time intervals of about 2 hr. I've tried to aline these three examples of sector boundaries so

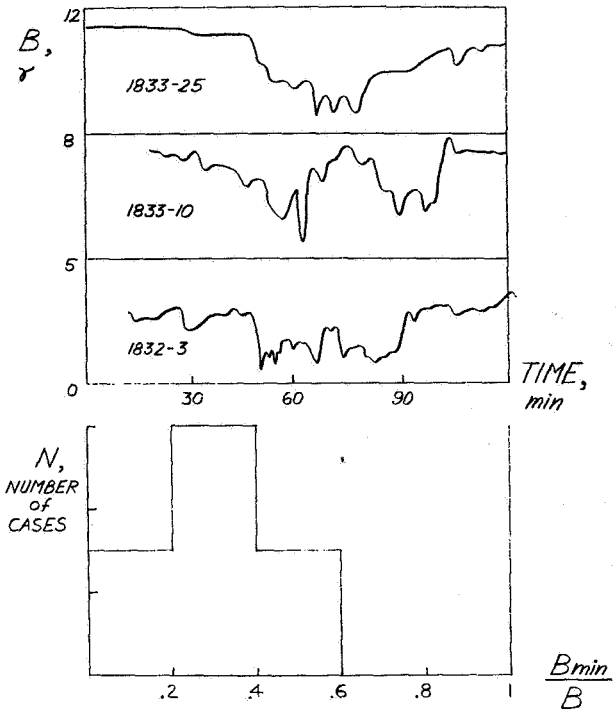

Figure 1. *Changes in interplanetary field magnitude at three sector boundaries.*

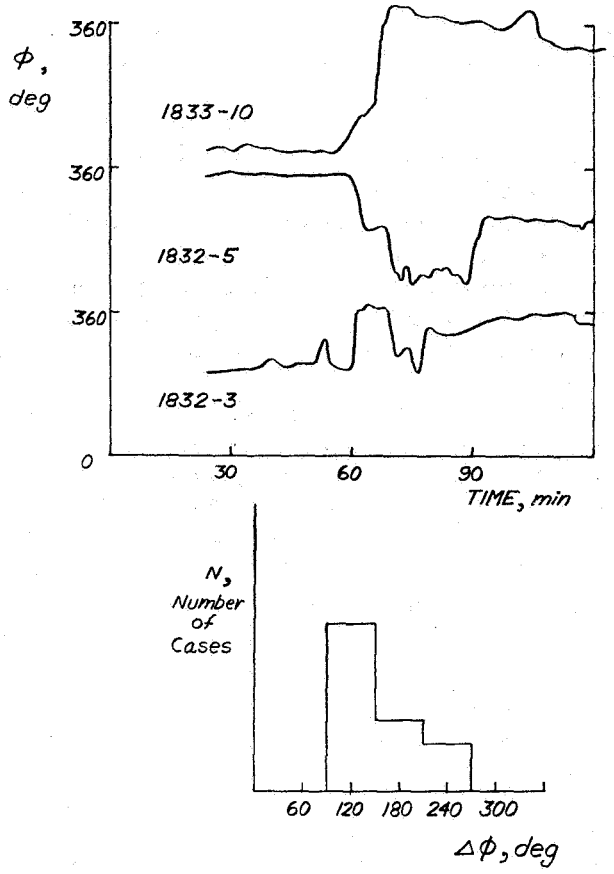

Figure 2. *Changes in the direction of the interplanetary field at three sector boundaries.*

that they can be compared. The identification numbers are our way of designating the sector boundaries in terms of the day number of solar rotation in which they occurred. The most obvious and interesting feature is the marked depression in the magnitude of the magnetic field. This is probably what most people have in mind when they think about the sector boundary as some kind of a simple neutral sheet.

The polarity usually changes in the vicinity of the magnitude change, but need not be coincident with it. On some occasions the direction of the field will start before the depression in the field and in some cases it will finish afterwards. In other cases the change in the field, particularly if it is an abrupt change in the direction of the field, can occur inside the field depression. There is certainly not a one-to-one correspondence between the two. Figure 2 shows some changes that tend to occupy somewhat different time intervals. The scales on the figure are variable because they were chosen at different times. They are 0 to 5γ, 0 to 8γ, and 0 to 12γ.

The histogram at the bottom of the figure shows the ratio of the minimum value to the magnitude of the field essentially ahead of the sector boundary. The differences in magnitude are not great on the two sides, and as you can see, the most probable value turns out to be about 0.3. This result is apparently similar to what is found in the earth's magnetotail where, based on published results, the field rarely ever goes to 0 but it is typically reduced to a value which is less than 40 percent of the magnetotail field. So far, so good.

Figure 2, then, gives us some examples and a histogram indicating how the field

direction changes. Each is scaled 360°–0 to 360° in each case. Some of the changes are very abrupt whereas others are quite slow. There is some irregularity; however, I am impressed by the result that the changes themselves are typically not 180°. One change is substantially larger, while two others are smaller, as shown more clearly by the histogram. The rotation of the magnetic field across the sector boundary is shown in intervals from 10 to 30 min. I should point out that these plots are in the principal axis system, so you're looking down on the plane in which the rotation of the field tends to occur. The histogram shows no particular preference for a change of 180° or for antiparallel, oppositely directed fields on the two sides of the sector boundary. In fact, there does seem to be more of a tendency for the angle through which the fields rotate to be less than 180°. I thought this was an intriguing observation and I would like to suggest an explanation for it.

Figure 3 illustrates the basic idea, which is relatively simple. It is based on the effect of a wind shear on the two sides of the sector boundary. The sector boundary is represented by the horizontal plane in this diagram. I have assumed a relative motion of the solar wind parallel to the sector boundary on the two sides. In this case the velocity is higher in the upper half of the figure. For the sake of illustration, I have also assumed a gradient in that direction. One can draw other configurations, but they simply indicate that wind shears of this kind would indeed lead to a displacement of the field line on one side of the sector boundary relative to it's location on the other.

Having looked at the Mariner plasma data, the existence of a velocity change across the sector boundary seems to be a very common kind of phenomena. This hypothesis is one which I have only been considering for only a short period of time, but since I have been here at this conference I have found that it is, of course, not a new idea. You may recall the other day that Professor Cowling made a comment about the concept of the neutral sheet. He asked at that time about the possibility of wind shears. I spoke to him about this afterward and he said that people who had worked on neutral sheet problems in connection with solar flares had found that in that case shearing motions were very important in many of their models. This is obviously just a hypothesis at this point; if it is borne out by more careful analysis, many of you who are interested in neutral sheets, sector boundaries, and such things as field-line merging may want to consider some of the implications of these shearing motions and of the fields not being simply antiparallel as they are in the earth's magnetotail.

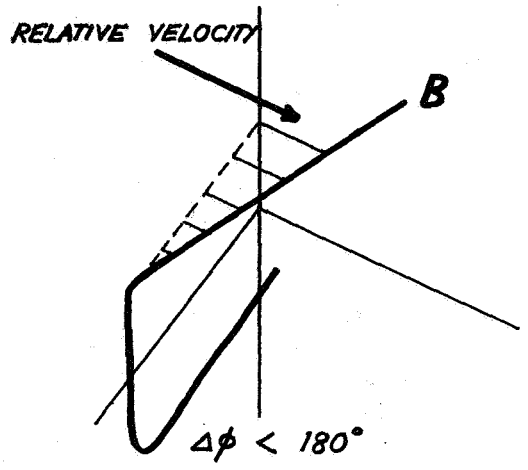

Figure 3. *Effect of a solar wind shear on the relative field direction on two sides of a sector boundary.*